Separation of source, site and near-surface attenuation effects in western Turkey

ARTICLE *in* NATURAL HAZARDS · FEBRUARY 2015

Impact Factor: 1.72 · DOI: 10.1007/s11069-015-1660-7

2 AUTHORS:

Tevfik Özgür Kurtulmuş

Dokuz Eylul University

16 PUBLICATIONS **101** CITATIONS

SEE PROFILE

Nihal Akyol

Dokuz Eylul University

13 PUBLICATIONS **165** CITATIONS

SEE PROFILE

Journal : Small 11069 | Dispatch : 12-2-2015 | Pages : 18
Article No. : 1660 | LE | TYPESET
MS Code : NHAZ-D-14-00285 | CP | DISK

Nat Hazards
DOI 10.1007/s11069-015-1660-7

ORIGINAL PAPER

Separation of source, site and near-surface attenuation effects in western Turkey

Tevfik Özgür Kurtulmuş · Nihal Akyol

Received: 18 March 2014 / Accepted: 10 February 2015

Abstract We analyzed 1764 records from 322 micro- and moderate-size local earthquakes in the central west Turkey to separate source, site and near-surface attenuation effects by utilizing a generalized inversion technique (GIT) to the spectra. GIT site transfer functions were compared with horizontal-to-vertical spectral ratio (HVSR) estimates by Akyol et al. (Pure Appl Geophys 170(12):2107–2125. doi: 10.1007/s00024-013-0661-2, 2013). Large amplitude values of vertical component GIT site transfer functions were obtained at different frequency bands for some of the sites. These results imply contaminations of HVSR estimates due to basin geometry induced waves caused by deep or shallow lateral heterogeneities. GIT source function estimates were interpreted as Brune source model. Weak epicentral dependence of near-surface attenuation parameter κ with large scattering could be attributed to the source and propagation path complexities along different paths arriving to the stations. Large f_e values with large κ_0 values emphasize near-surface weathered zones attenuation effect at high frequencies.

Keywords Site function · Generalized inversion technique · Source function · Near-surface attenuation · Kappa parameter · Western Turkey

1 Introduction

Although the origin, timing of initiation, geometry and evolution of the major extensional features is still debated, it is known that post-collisional extension in the Aegean extensional province caused several Alpine metamorphic massifs to be exhumed. One of them is the Menderes Massif (e.g., Gessner et al. 2001; Seyitoğlu and Işık 2009) where high-grade metamorphic rocks of the middle to lower crust are now exposed in the central west

T. Ö. Kurtulmuş (✉) · N. Akyol
Department of Geophysical Engineering, Faculty of Engineering, Dokuz Eylül University, Tınaztepe Campus, 35397 Buca, Izmir, Turkey
e-mail: ozgur.kurtulmus@deu.edu.tr

Journal : Small 11069 | Dispatch : 12-2-2015 | Pages : 18
Article No. : 1660 | LE | TYPESET
MS Code : NHAZ-D-14-00285 | CP | DISK

Turkey. Extension in the mid- and upper crust is mainly accommodated by large displacement along low-angle detachment faults (Hetzel et al. 1995; Gessner et al. 2001). Extensional deformation of the crust with increasing lithospheric thinning has been characterized by intense seismic activity (e.g., Taymaz et al. 1991; Le Pichon et al. 1995), extensive volcanism (e.g., Tokçaer et al. 2005; Aldanmaz 2006), mineralization (e.g., Sayın 2007; Yılmaz 2007), geothermal systems (e.g., Tarcan et al. 2000; Mutlu 2007), the high heat flow (e.g., İlkışık 1995; Göktürkler et al. 2003) and low Pn values (e.g., Al-Lazki et al. 2004; Mutlu and Karabulut 2011) around the horst–graben system in western Turkey. Approximately E–W trending the Gediz, Küçük Menderes and Büyük Menderes grabens, separated by the Bozdağ and Aydın Mountain Horsts, are the most prominent neotectonic features of the region (Fig. 1). The Gediz and the Büyük Menderes grabens contain deep sedimentary sequences with thicknesses being more than 3000 m in some localities (e.g., Sarı and Şalk 2006; Çiftçi

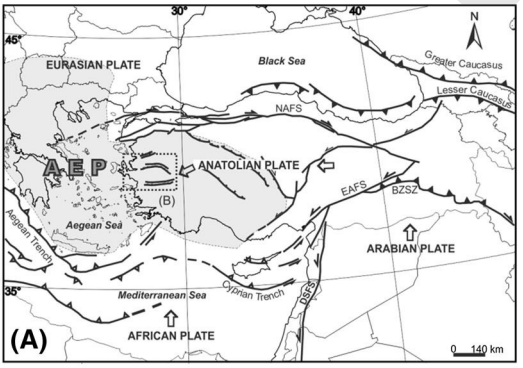

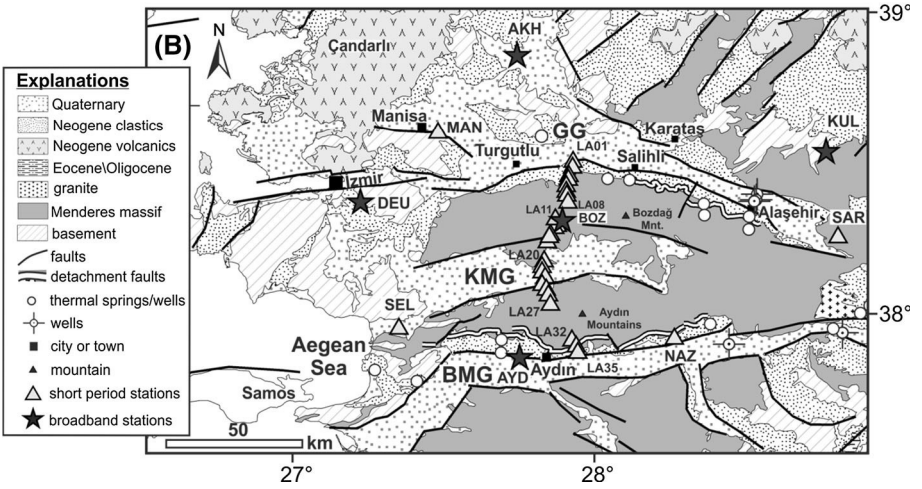

Fig. 1 **a** Simplified tectonic map of Turkey showing major neotectonic structures (after Çiftçi et al. 2010). **b** Simplified geologic map of the central west Turkey (after Çiftçi et al. 2010). The location of **b** is marked in **a** as a *dotted box*. *NAFS* North Anatolia fault system, *EAFS* East Anatolia fault system, *BZSZ* Bitlis Zagros suture zone, *DSFS* dead sea fault system, *EG* Edremit graben, *BçG* Bakırçay graben, *GG* Gediz graben, *KMG* Küçük Menderes graben, *BMG* Büyük Menderes graben, *DG* Denizli graben, *SG* Simav graben. *White triangles* and *blue stars* indicate short-period and broadband stations, respectively, used in this study (after Akyol et al. 2013)

Journal : Small 11069 | Dispatch : 12-2-2015 | Pages : 18
Article No. : 1660 | LE | TYPESET
MS Code : NHAZ-D-14-00285 | CP | DISK

and Bozkurt 2009; Çiftçi et al. 2010). The Küçük Menderes graben is younger than the others (Rojay et al. 2005), and sedimentary thickness is up to 270 m.

Because of high seismicity accommodating crustal deformation and stratigraphic conditions, on which have, urbanized and industrialized large cities in western Turkey, the importance of site-specific seismic hazard assessments becomes more crucial. Characterizing source, site and path effects is important for both assessing the seismic hazard in a specific region and generation of the building codes or renewing previous ones. The detailed knowledge of the expected spectral ground motion models permits us simulating time histories of possible earthquakes and design of earthquake-resistant structures at a site of interest (Oth 2007). The common approach to separate the earthquake source processes, path effects and site amplification is to apply the generalized inversion technique (GIT) to the recorded ground motion data. GIT was first proposed by Andrews (1986) and developed by many researchers with different algorithms (e.g., Castro et al. 1990; Boatwright et al. 1991; Hartzell 1992). One of the empirical methodologies commonly used for site effect assessment is non-reference station technique which is also called as Nakamura (Nakamura 1989) or 'horizontal to vertical spectral ratio (HVSR).' This method hypothesizes that the vertical component of motion is amplification free and not influenced by the local structure, whereas the horizontal components contain P-to-S conversions due to the local geological features around the station (Parolai et al. 2004). The main goal of this study was to obtain source, site and near-surface attenuation effects from the spectra, for the central west Turkey. After eliminating nonparametric attenuation function effect (Kurtulmuş 2014), we decomposed source and site spectral functions of micro- and moderate-size earthquakes. Then we compared GIT site functions with the HVSR estimates by Akyol et al. (2013) to examine whether or not there is any vertical motion site transfer function contamination effect on the results. The near-surface attenuation effect of each site was also evaluated utilizing the original method of Anderson and Hough (1984).

2 Data

We used 1764 records from 322 micro- and moderate-size local earthquakes with the magnitude range of $2.0 < M_L < 5.6$ in western Turkey. The data come from the Western Anatolia Seismic Recording Experiment (WASRE) network (Akyol et al. 2006; Zhu et al. 2006) which has two different array configurations (Fig. 1). The first one is a linear array (LA) which traversed the Gediz graben (GG), the Büyük Menderes graben (BMG) and the Küçük Menderes graben (KMG) with a station spacing of 3–4 km: Twenty of the short-period instruments (ranging from stations LA01 to LA20) were first deployed for $\sim$5.5 months along $\sim$50-km-long N–S line, and then, eighteen of them were redeployed (ranging from stations LA21 to LA38) for the remaining $\sim$5.5 months, to extend the array southward. The geological cross section along the linear array stations was given by Akyol et al. (2013). Stations LA01 and LA20 were deployed during whole data acquisition stage together with the regional array which surrounds the linear array (Fig. 1) and consists of four short-period (MAN, NAZ, SAR and SEL) and five broadband instrument stations (AKH, AYD, BOZ, DEU and KUL). The station list including geological units on which they were deployed was given in Table 1 (after Akyol et al. 2013). The data were collected by 5 STS-2 broadband and 24 Mark L-22 short-period (2 Hz) instruments, in between November 2002 and October 2003. Figures 2 and 3 show the network configuration and data distribution (after Kurtulmuş and Akyol 2013), and the source-to-station path coverage used in this study, respectively. Local magnitude distributions (ranging from 2.0 to 5.6)

Table 1 List of codes, coordinates, site formation (after Akyol et al. 2013) and obtained average values of f_e, κ and κ_0 for each station

Station code	Latitude (N)	Longitude (E)	Elevation (m)	Site formation	$f_e \pm$ SD	Ave. $\kappa \pm$ SD	$\kappa_0 \pm$ SE	SE of fit	SL of fit
LA01	38.4987	28.1135	130	Alluvium	5.98 (±1.52)	0.036 (±0.006)	0.034 (±0.002)	0.006	0.207
LA03 (39)	38.4497	28.1136	309	Neogene conglomerate	7.23 (±1.86)	0.024 (±0.010)	0.019 (±0.006)	0.010	0.388
LA04	38.4428	28.0915	654	Neogene conglomerate	6.23 (±0.96)	0.046 (±0.009)	0.036 (±0.005)	0.009	0.023
LA05	38.4288	28.0903	802	Micaschist	7.47 (±1.34)	0.019 (±0.008)	0.015 (±0.005)	0.008	0.455
LA06	38.4036	28.0804	1043	Micaschist	7.51 (±1.33)	0.034 (±0.008)	0.026 (±0.009)	0.090	0.396
LA07	38.3805	28.0793	1093	Micaschist	6.60 (±1.42)	0.024 (±0.009)	0.016 (±0.003)	0.009	0.007
LA13	38.2956	28.0213	989	Micaschist	7.80 (±1.56)	0.044 (±0.010)	0.029 (±0.004)	0.009	0.003
LA15 (40)	38.2593	27.9947	244	Micaschist	8.44 (±1.45)	0.028 (±0.012)	0.042 (±0.009)	0.011	0.105
LA16	38.2391	27.9835	186	Alluvium and micaschist	6.81 (±1.77)	0.042 (±0.011)	0.038 (±0.005)	0.011	0.379
LA20	38.1841	27.9687	129	Micaschist	4.88 (±1.46)	0.038 (±0.010)	0.030 (±0.003)	0.010	0.010
LA21	38.1619	27.9573	127	Micaschist	6.02 (±1.50)	0.046 (±0.009)	0.040 (±0.007)	0.009	0.424
LA22	38.1404	27.9582	169	Gneissic granite	8.07 (±1.94)	0.027 (±0.011)	0.022 (±0.004)	0.011	0.270
LA23	38.1196	27.9748	231	Gneissic granite	6.92 (±2.18)	0.040 (±0.010)	0.023 (±0.009)	0.009	0.064
LA26	38.0495	27.9891	985	Micaschist	7.44 (±2.05)	0.042 (±0.010)	0.046 (±0.004)	0.010	0.034
LA27	38.0301	27.9929	753	Micaschist	7.85 (±2.06)	0025 (±0.011)	0.0259 (±0.008)	0.012	0.923
LA32	37.9148	28.0514	280	Sandstone	6.60 (±2.22)	0.031 (±0.009)	0.028 (±0.008)	0.009	0.676
LA33	37.8937	28.0439	226	Sandstone	8.20 (±1.38)	0.035 (±0.011)	0.027 (±0.006)	0.011	0.145
LA34	37.8692	28.0524	142	Sandstone and conglomerate	6.96 (±1.56)	0.033 (±0.012)	0.017 (±0.005)	0.010	0.002
AKH*	38.9149	27.8081	128	Alluvium	7.67 (±1.46)	0.050 (±0.013)	0.048 (±0.006)	0.013	0.805
AYD*	37.8407	27.8374	86	Alluvium	6.75 (±1.90)	0.033 (±0.011)	0.034 (±0.004)	0.011	0.892
BOZ*	38.3002	28.0495	1216	Agricultural soil on top of the micaschist	8.70 (±1.00)	0.033 (±0.007)	0.029 (±0.002)	0.007	0.092
DEU*	38.3710	27.2078	248	Limestone	6.84 (±1.86)	0.037 (±0.012)	0.034 (±0.002)	0.012	0.039
KUL*	38.5401	28.6339	700	Agricultural soil on top of the micaschist	6.19 (±1.89)	0.032 (±0.011)	0.027 (±0.006)	0.011	0.290

Journal : Small 11069
Article No. : 1660
MS Code : NHAZ-D-14-00285
Dispatch : 12-2-2015
Pages : 18
LE
CP
TYPESET
DISK
Nat Hazards

Table 1 continued

Station code	Latitude (N)	Longitude (E)	Elevation (m)	Site formation	$f_e \pm$ SD	Ave. $\kappa \pm$ SD	$\kappa_0 \pm$ SE	SE of fit	SL of fit
MAN	38.5931	27.5184	88	Alluvium and colluvium	6.88 (±1.75)	0.038 (±0.011)	0.034 (±0.003)	0.011	0.123
NAZ	37.9134	28.3432	119	Alluvium	7.81 (±2.04)	0.049 (±0.013)	0.038 (±0.010)	0.013	0.229
SAR	38.2345	28.6859	279	Sandstone	7.43 (±1.85)	0.039 (±0.012)	0.036 (±0.002)	0.012	0.130
SEL	37.9443	27.3677	49	Alluvium	7.00 (±1.60)	0.042 (±0.015)	0.041 (±0.005)	0.015	0.813

SD standard deviation, *SE* standard error and *SL* significance level from *F* test

* Represents broadband stations

Nat Hazards

Journal : Small 11069 Dispatch : 12-2-2015 Pages : 18
Article No. : 1660 ☐ LE ☐ TYPESET
MS Code : NHAZ-D-14-00285 ☑ CP ☑ DISK

Journal : Small 11069 | Dispatch : 12-2-2015 | Pages : 18
Article No. : 1660 | LE | TYPESET
MS Code : NHAZ-D-14-00285 | CP | DISK

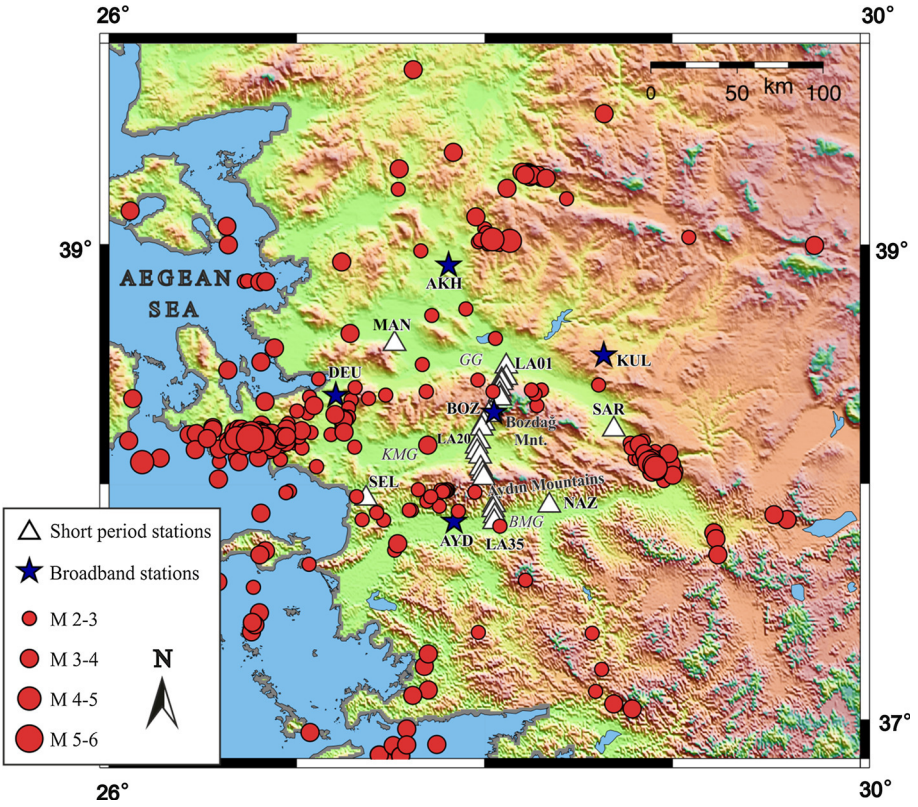

Fig. 2 Locations of the stations and distribution of earthquakes (*red dots*) used in this study. *White triangles* and *blue stars* indicate short-period and broadband stations, respectively. *GG* Gediz graben, *KMG* Küçük Menderes graben, *BMG* Büyük Menderes graben (after Kurtulmuş and Akyol 2013)

versus hypocentral distances (ranging from 3.5 to 205 km) and focal depths (ranging from 1.4 to 27 km) can be seen in Kurtulmuş and Akyol (2013). The detail about initial data processing stages were given by Akyol et al. (2013). Briefly, S-wave portions of radial (*R*), transverse (*T*) and vertical (*V*) components were selected with a duration of 7 s, and Fourier transform was computed after applying a 5 % cosine tapered window. The spectra were smoothed with a 9-point moving average operator. This dataset was used for site transfer function estimations, utilizing 'standard spectral ratio (SSR)' and HVSR techniques, to highlight site-specific seismic hazard potential of deep basin structures and for examining crustal attenuation characteristics by parameterizing nonparametric attenuation functions, in the region (Akyol et al. 2013; Kurtulmuş and Akyol 2013; Kurtulmuş 2014).

3 Method and results

3.1 Separation of source and site effects

The amplitude spectrum of a ground motion observed at a site *j* from an event *i* can be expressed (e.g., Castro et al. 1990, 2004) as following:

Journal : Small 11069 | Dispatch : 12-2-2015 | Pages : 18
Article No. : 1660 | LE | TYPESET
MS Code : NHAZ-D-14-00285 | CP | DISK

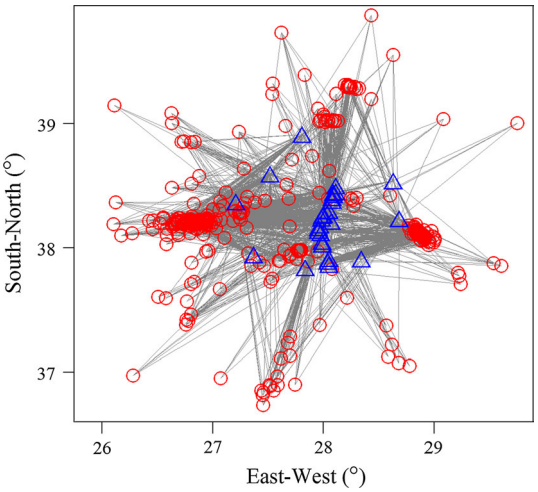

Fig. 3 Schematic source-to-station ray path coverage of the dataset. *Red circles* and *blue triangles* represent the events and stations, respectively

$$U_{ij}(f,r) = S_i(f)A_{ij}(f,r)Z_j(f) \tag{1}$$

where $S_i(f)$ denotes the source function, $A_{ij}(f,r)$ is the attenuation effect along the hypocentral distance r, and $Z_j(f)$ is the local site function. The nonparametric attenuation functions, including anelasticity of heterogeneous media and geometrical spreading effects, were obtained for 26 different frequencies between 0.3 and 19.7 Hz for three components (Kurtulmuş 2014). To separate source and site functions, these total attenuation effects were removed from the data as follows:

$$U_{ij}^{A}(f) = \frac{U_{ij}(f,r)}{A_{ij}(f,r)} = S_i(f)Z_j(f) \tag{2}$$

By taking the logarithm, the problem can be linearized and Eq. (2) can be written for a fixed frequency f;

$$d_{ij} = s_i + z_j \tag{3}$$

Herein, $d_{ij} = \log U_{ij}^{A}(f)$ is the logarithm of the corrected spectral amplitude, $s_i = \log S_i(f)$ and $z_j = \log Z_j(f)$ are logarithmic source and site functions, respectively. Singular value decomposition method (Menke 1989) is used to solve this linear system for three components. To overcome the linear dependence problem between the source and site terms (e.g., Andrews 1986; Castro et al. 1990, 2003; Oth et al. 2009), either constrained-source or constrained-site spectral function should be used in the inversion. In this study, we used following constraint:

$$\sum_{j=1}^{N} \log Z_j(f) = 0 \tag{4}$$

where N is equal to the number of reference site stations. Here, stations LA13, LA22 and MAN were chosen as reference sites according to the results of HVSR estimates by Akyol et al. (2013), which show the lowest site amplification. Obtained site functions of the

Journal : Small 11069 | Dispatch : 12-2-2015 | Pages : 18
Article No. : 1660 | LE | TYPESET
MS Code : NHAZ-D-14-00285 | CP | DISK

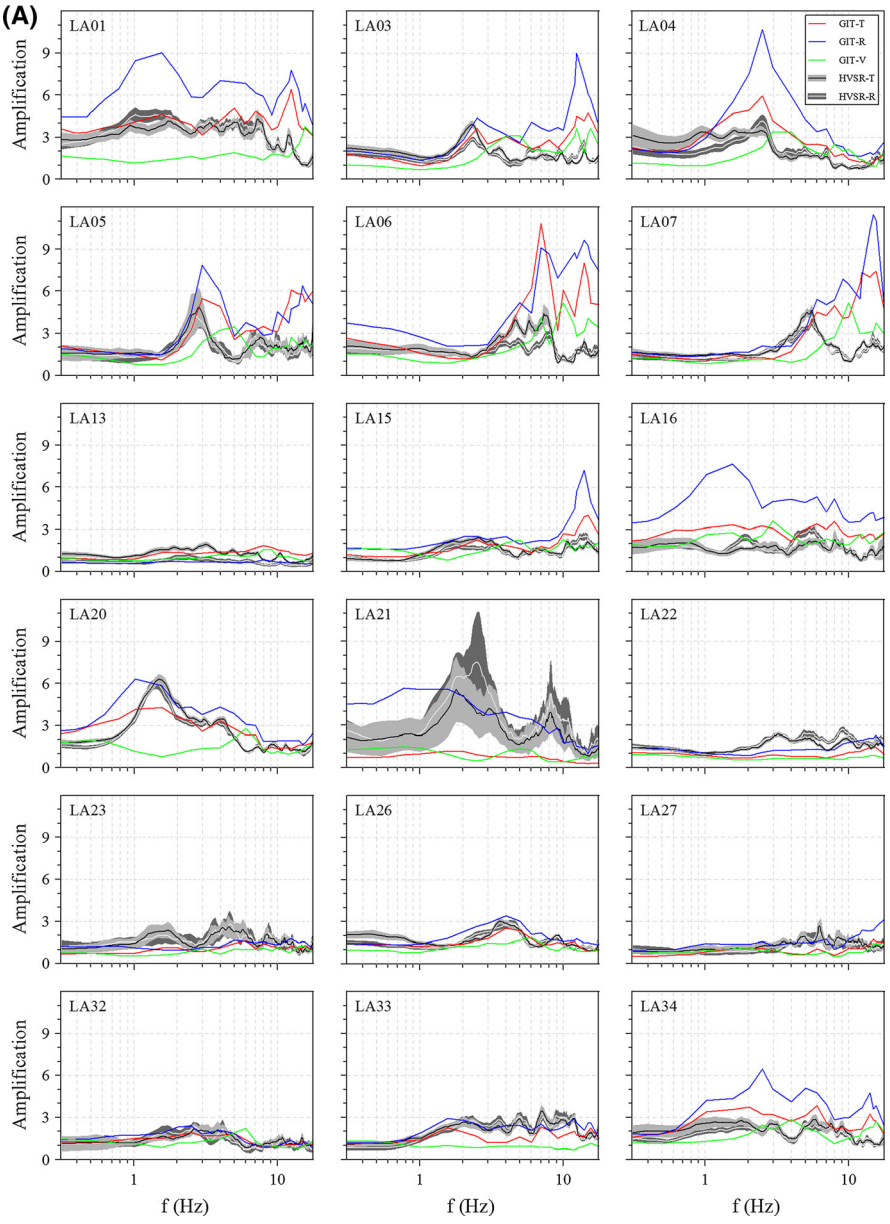

Fig. 4 **a** GIT site functions from three components for the linear array stations together with HVSR estimates. *Red*, *blue* and *green lines* represent GIT site functions for *T*-, *R*- and *V*-components, respectively. RMS values of the residuals associated with the inversion step are given in Fig. 5. *Black* and *white lines* represent the average HVSR estimates for *T*- and *R*-components, respectively, together with 90 % confidence interval (after Akyol et al. 2013). **b** GIT site functions from three components for the regional array stations together with HVSR estimates. *Red*, *blue* and *green lines* represent GIT site functions for *T*-, *R*- and *V*-components, respectively. RMS values of the residuals associated with the inversion step are given in Fig. 5. *Black* and *white lines* represent the average HVSR estimates for *T*- and *R*-components, respectively, together with 90 % confidence interval (after Akyol et al. 2013)

Journal : Small 11069 | Dispatch : 12-2-2015 | Pages : 18
Article No. : 1660 | LE | TYPESET
MS Code : NHAZ-D-14-00285 | CP | DISK

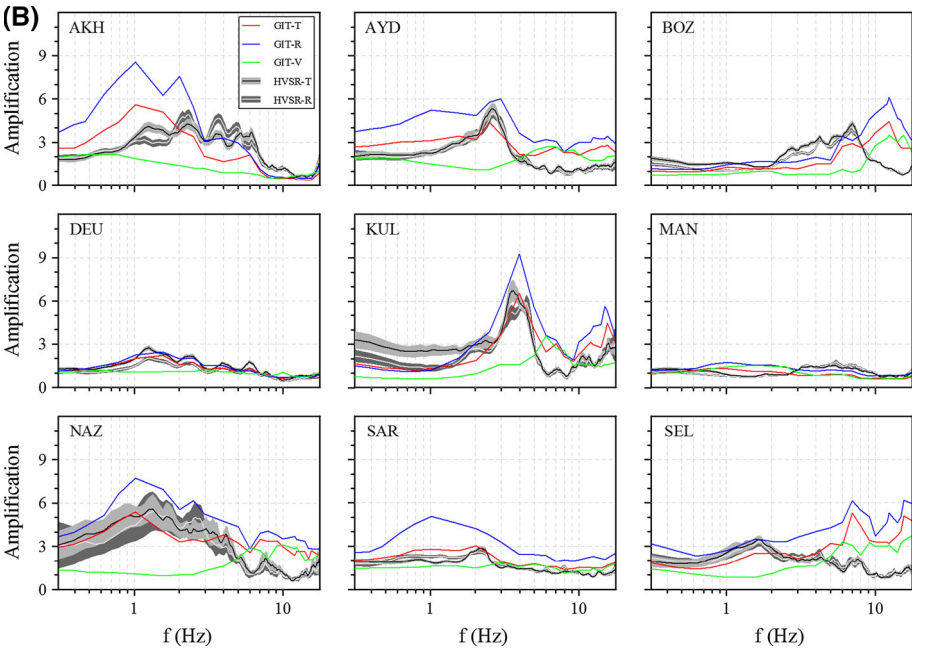

Fig. 4 continued

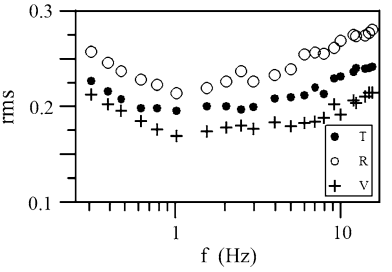

Fig. 5 RMS values of the residuals associated with GIT step, separating source and site functions

stations were given in Fig. 4, in order to compare, together with these HVSR estimates. RMS values of the residuals associated with the inversion results are given in Fig. 5. Figure 6 shows GIT spectral source function estimates from three components.

3.2 Near-surface attenuation effects

Originally, the parameter kappa (κ) to define the near-surface attenuation was introduced by Anderson and Hough (1984). This parameter describes the asymptotic high-frequency slope of the spectra (Kilb et al. 2012). The spectrum exponentially decaying at high frequencies was parameterized as follows (Anderson and Hough 1984):

$$A(f) = A_0 e^{-\pi f}, \quad f > f_e \tag{5}$$

where A_0 is a source- and propagation path-dependent amplitude, κ is the spectral decay parameter which accounts for the attenuation along the path near the site, and f_e is the frequency above which the spectral amplitude follows an exponential decay.

Journal : Small 11069 | Dispatch : 12-2-2015 | Pages : 18
Article No. : 1660 | LE | TYPESET
MS Code : NHAZ-D-14-00285 | CP | DISK

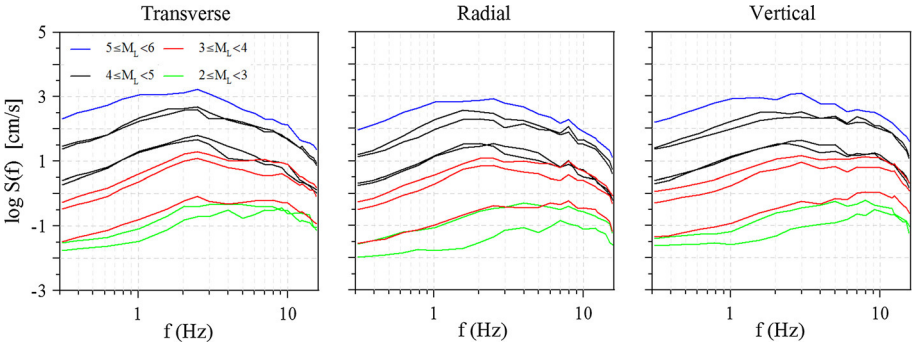

Fig. 6 Examples from GIT source functions estimated for three components

Because of its empirical nature, the debate on the origin and physical meaning of this parameter still continues (Ktenidou et al. 2013): Some researches correlate it to the seismic source (e.g., Malagnini et al. 2002; Halldorsson and Papageorgiou 2005; Iwakiri and Hoshiba 2012), whereas others relate it to the site effects (e.g., Petukhin and Irikura 2000; Cotton et al. 2006; Drouet et al. 2010). For instance, Anderson and Hough (1984) interpreted that κ was affected for amplitude reductions near the surface due to variations in the geologic conditions under the recording stations. Some authors also have suggested an alternative model that it is a combination of near-surface attenuation and source effect (e.g., Tsai and Chen 2000; Purvance and Anderson 2003). Douglas et al. (2010) calculated kappa from the original strong motion records, utilizing Anderson and Hough (1984) approach. Assuming a negligible dependence of geometrical spreading on frequency, Gentili and Franceschina (2011) estimated κ after correcting the spectra for the frequency dependent part of the quality factor. As an alternative model, Bindi et al. (2006) estimated kappa by decomposing source, site and distance effects on the high-frequency part of the spectra. Detailed discussion on taxonomy of kappa has been given by Ktenidou et al. (2014).

In this study, kappa values were estimated after eliminating the effects of an average nonparametric attenuation function and ω^2 source model, inferred from Eqs. (1) and (2), respectively (e.g., Castro et al. 2000). κ parameter has been calculated from T-component spectrum of each record, utilizing Eq. (5), through a linear regression between f_e and the frequency at which the noise level starts contaminating the signal. At high frequencies larger than the corner frequency, the fall of the spectral amplitudes was modeled by ω^2 source model, regarding GIT source function estimates. Here, we used an algorithm based on searching the minimum error, by trying every frequency above which the spectral amplitude follows an exponential decay, as an initial point of the linear least-squares fit. The lower limit of the frequency bandwidth for the linear regression was adopted as larger than corner frequency and it changes depending on event size. All of the processes were verified visually. On the other hand, the corner frequency can be underestimated due to a severe near-surface attenuation effect on the spectral shape (e.g., Anderson 1986; Abercrombie and Leary 1993). Figure 7 shows an example for computing κ from the corrected spectrum. After that, we plotted κ values of each record as a function of epicentral distance for each station. The linear dependence between κ and epicentral distance at each station was also examined as follows (Anderson and Hough 1984):

Journal : Small 11069 | Dispatch : 12-2-2015 | Pages : 18
Article No. : 1660 | LE | TYPESET
MS Code : NHAZ-D-14-00285 | CP | DISK

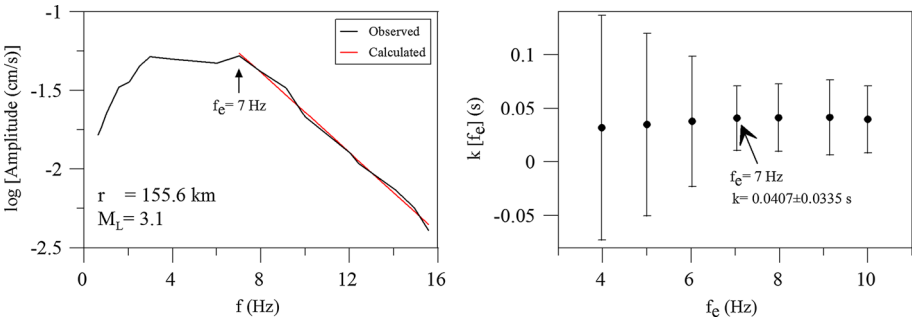

Fig. 7 An example for computing κ from the corrected spectrum (*left*). κ estimates and corresponding standard deviations as a function of initial point adopted for the linear regression (*right*). The best estimate of κ and the corresponding value of f_e are indicated by an *arrow*

$$\kappa(r) = \kappa_0 + \tilde{\kappa}(r) \tag{6}$$

in which r is the epicentral distance. Therefore, the distance dependence can be eliminated by extrapolating the $\tilde{\kappa}(r) = \frac{d\kappa}{dr} r$ trend to $r = 0$. A site-specific kappa, typically denoted as κ_0, is thought to be free of the regional Q attenuation effect. Obtained average values of f_e, κ and κ_0 for each station can be seen in Table 1. Figure 8 shows the variation of κ values with distance and κ_0 estimates for each site.

4 Discussions

We used 1764 records from 322 micro- and moderate-size local earthquakes in the central west Turkey to separate source, site and near-surface attenuation effects. GIT site function estimates were given in Fig. 4, together with HVSR estimates by Akyol et al. (2013). This figure represents HVSR estimates calculated for the radial to vertical (R/V) and transversal to vertical (T/V) components. Black and white lines represent the average HVSR estimates for T- and R-ones, respectively. As shown in this figure, large amplitude values of V-component GIT site estimates were observed at varying frequency ranges for different stations. This means that the vertical component of motion is influenced by the local structure and causes contamination of spectral ratio site estimates. Two-dimensional or 3D effects and low impedance contrast between sediments and basement can preclude HVSR applications (Yalçınkaya et al. 2013). Malagnini et al. (2004) have suggested that the vertical motion transfer function is not amplification free and HVSR does not represent the characteristics of the true horizontal site transfer function. Similarly, Castro et al. (2004) stated that vertical amplification can be significant (up to a factor of 25) and consequently HVSR may underestimate the site response. GIT site amplitude values of radial components are larger than transverse ones, especially for the stations located on young and deep sedimentary fill, such as LA01, LA20, LA21, AKH, AYD and NAZ sites (Fig. 4). This could be explained by P-to-S conversion at the bedrock/soil layer contact (Parolai et al. 2004). The differences in the amplitude values from different techniques may arise from complexities in the wave field due to constructive/destructive interference, diffraction and scattering (Parolai et al. 2004). Cornou et al. (2003) pointed out the importance of sediment–bedrock interface and structure geometry which control frequency input motion in

AQ1

Journal : Small 11069 | Dispatch : 12-2-2015 | Pages : 18
Article No. : 1660 | LE | TYPESET
MS Code : NHAZ-D-14-00285 | CP | DISK

shaping wave fields. Qin et al. (2012) demonstrated that 3D basin geometry causes a wavefront focusing effect and contributes significantly to a localized strong amplification.

Although shallow heterogeneities resulting from varying degrees of weathering or cracking of the rock cause the velocity decrease near surface, the reference rock site

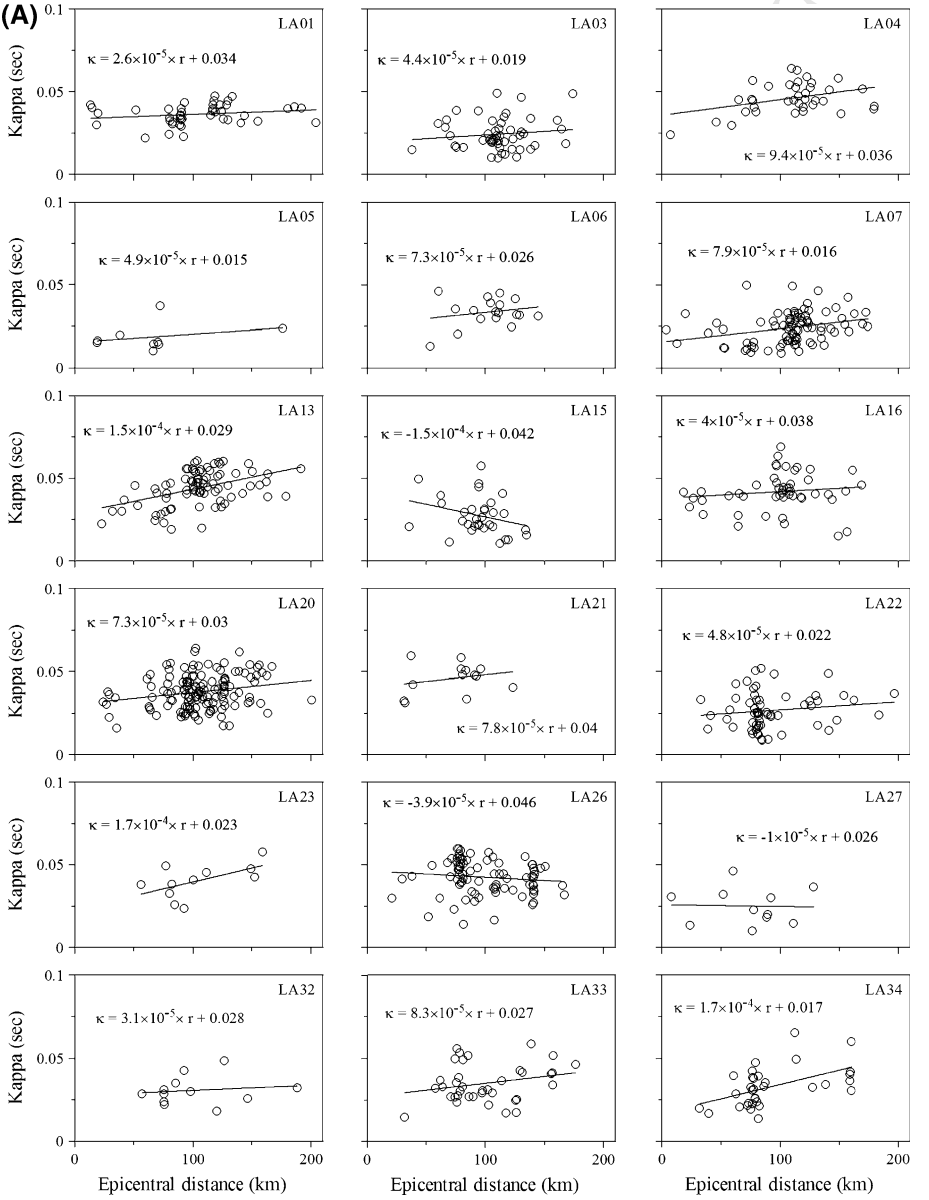

Fig. 8 **a** κ values versus epicentral distance for linear array stations. Equations of linear least-square fits (*solid lines*) are given for each site. **b** κ values versus epicentral distance for regional array stations. Equations of linear least-square fits (*solid lines*) are given for each site

Journal : Small 11069 | Dispatch : 12-2-2015 | Pages : 18
Article No. : 1660 | LE | TYPESET
MS Code : NHAZ-D-14-00285 | CP | DISK

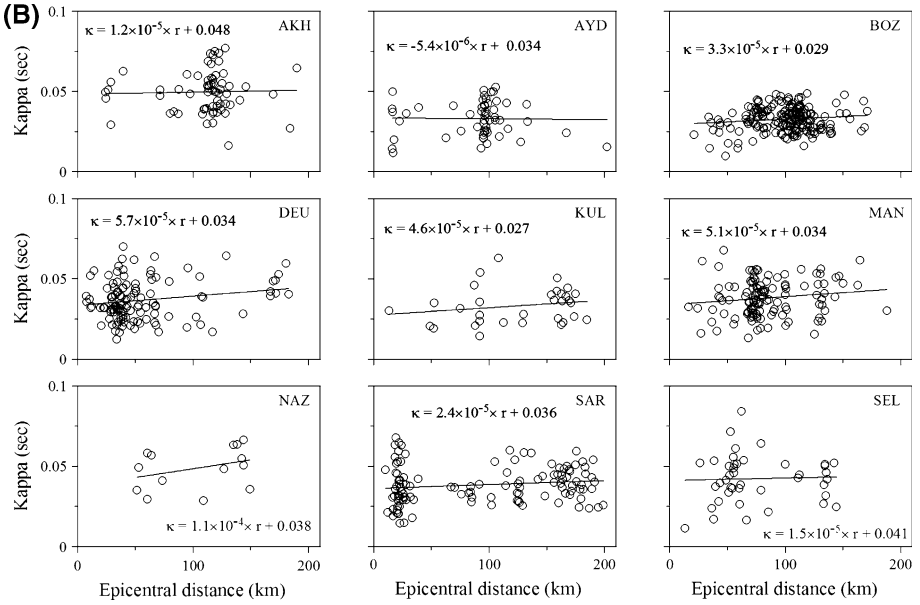

Fig. 8 continued

definition is needed for probabilistic seismic hazard assessment. According to *V*-component GIT site functions in Fig. 4, only stations LA13, LA22, LA23, LA26, LA27, LA33, DEU and MAN could be considered as reference sites. Large RMS residuals associated with the inversion results (Fig. 5) imply more contamination on the *R*-component. *V*-component RMS residuals are smaller than the other components at the frequencies larger than 1 Hz. It might imply that the vertical component of motion is less influenced by the local structure, whereas the horizontal components contain the P-to-S conversions due to the local geological features around the station (Parolai et al. 2004).

Figure 6 represents GIT spectral source function estimates from each component. Here, we used the unconstrained-source spectral shape and the constrained-site response methodology. Although most of the source functions have slight fall off at high frequencies as predicted by simple dislocation model, GIT source function estimates were interpreted as ω^2 source model (Brune 1970) which is reasonable for micro- and moderate-size earthquakes.

After eliminating source and attenuation effects, near-surface attenuation parameter, κ, was estimated from *T*-component spectra for each site (Table 1). Weak distance dependencies of κ values were observed. The absence of a statistically significant dependence of κ on the distance has been reported by different works (e.g., Castro et al. 2000; Purvance and Anderson 2003; Fernández et al. 2010). Examining the events within a radius of 2.5 km, Castro et al. (2000) have concluded that the great variability of κ values for similar source–station paths is partially due to complexity of near source and also differences in source parameters. In Fig. 8b, the κ values for the distance closer than 50 km come from the same cluster for the SAR stations. Similarly, obtained κ values with large scattering for narrow bands of distance in Fig. 8 are related to clustering events shown in Fig. 2. On the other hand, BOZ station is in the middle of the region with the best azimuthal data distribution. Thus, large scattering on κ estimates for this station implies changing

Journal : Small 11069 | Dispatch : 12-2-2015 | Pages : 18
Article No. : 1660 | LE | TYPESET
MS Code : NHAZ-D-14-00285 | CP | DISK

attenuation values along different paths due to structural complexity in the region. Note that, we eliminated nonparametric attenuation functions from the spectra. $A_{ij}(f,r)$ functions represent average attenuation for the region without any azimuthal information contained in each recording. Another possibility is that the site response may be responsible for the scattering of κ values, since site amplification can also modify the shape of the spectra (Castro et al. 2000). For that reason, in our results, variability of κ values could be related with not only source but also whole propagation path effects.

Generally, κ_0 is considered to be the near-surface attenuation effect of seismic waves beneath the station and that it depends on the site conditions. Here, grouping of kappa values according to the site conditions could not be derived, since we were not able to classify the sites. Although a reliable correlation between κ_0 and geological/geophysical characteristics of a site of interest has still been debated, many field studies present that κ_0 is generally smaller for rock sites than for the sites on alluvium and it can be used as an indicator of site effect (e.g., Castro et al. 1995; Atkinson 1996; Akyol et al. 2002). On the other hand, chosen frequency band effects on the results were discussed by some researchers (e.g., Liu et al. 1994; Parolai and Bindi 2004). Kilb et al. (2012) have stated that low values of κ ($\sim$5 ms) correspond to seismograms with a lot of high-frequency energy, whereas high values of κ ($\sim$40 ms) correspond to seismograms with a minimal amount of high-frequency energy. Fernández et al. (2010) suggested that κ_0 depends not only on the rock type, but also the degree of fracturing and erosion of the rocks near the recording sites. We could not evaluate the relation between κ_0 values and the degree of fracturing/erosion near the sites, due to lacking of any controlled experiment such as rock mechanics laboratory tests.

In this study, obtained minimum and maximum values of κ_0 are 0.015 and 0.049 s for the stations LA05 and AKH, respectively. Station LA05 is located on micaschist unit on the northern slope of the Bozdağ Horst, while station AKH is located on the alluvial unit of Akhisar Basin (thickness unknown). Similarly, Bindi et al. (2006) obtained κ_0 values smaller than 0.02 s for rock sites, while 0.036 and 0.042 s for two stations installed over the thick sedimentary fill in northwestern Turkey. Eyidoğan and Akıncı (1999) calculated κ parameter varied in the range of 0.0124–0.0364 s, and the average was 0.0246 ($\pm$0.0047) s in Erzincan, eastern Turkey. Castro et al. (1996) estimated the near-surface attenuation in the Friuli region, Italy, and obtained that the average κ_0 value is 0.03 s. Fernández et al. (2010) calculated κ in northeastern Sonora, Mexico, and found that the average κ_0 over the network of 0.04 s. Akıncı et al. (2013) scaled ground motions for western Turkey. They modeled an array average of near-surface attenuation values as in the excitation terms which depends on source characteristics such as the energy released. Their dataset contains our study area and dataset as a subset. They modeled the excitation term by using a Brune source model with a stress drop of 10 MPa for the largest event ($M_w = 5.8$) of the dataset with κ parameter of 0.045 s. When we averaged out κ_0 values of 27 different sites, an array average κ_0 is 0.031 ($\pm$0.009) s for our dataset.

Additionally, some of the stations such as LA15, LA26 and BOZ have large κ_0 values with large f_e values. These results could emphasize that near-surface alteration affects these recording sites. Obtained f_e values range between 4.88 and 8.7 Hz with an average value of 7.12 ($\pm$0.85) Hz. The minimum and maximum values are obtained for stations LA20 and BOZ, respectively. Station LA20 is located on the Küçük Menderes graben, while station BOZ is located on the Bozdağ horst. On the other hand, large f_e values with large κ_0 values were obtained for some of the sites which have significant amplification values on deep sedimentary units, such as stations AKH and NAZ. Large f_e values with large κ_0 values emphasize attenuation effects at high frequencies caused by near-surface weathered zones.

Journal : Small 11069 | Dispatch : 12-2-2015 | Pages : 18
Article No. : 1660 | LE | TYPESET
MS Code : NHAZ-D-14-00285 | CP | DISK

5 Conclusions

Spectral source and site functions were obtained for 322 events and 27 different locations in the central west Turkey, utilizing GIT. Significant *V*-component GIT site transfer functions for some of the stations imply contamination of HVSR estimates (Akyol et al. 2013) at different frequency bands, which could be related to complexities in the wave field caused by deep or shallow heterogeneities in the region such as differences in the basin geometries, fracturing and fluid saturation along different propagation paths. Obtained GIT source function estimates were interpreted as Brune source model. After eliminating source and attenuation function effects, we obtained an array average near-surface attenuation parameter κ_0 value as 0.031 ($\pm$0.009) s for the region. The minimum κ_0 value is 0.015 s for the station LA05 located on micaschist unit on the northern slope of the Bozdağ horst, while the maximum κ_0 value is 0.049 s for the station AKH located on the alluvial unit of deep sedimentary basin. Weak epicentral dependence of κ values could be attributed not only to near source but also to propagation path effects. For some of the stations located on shallow sedimentary deposits or horst, large f_e values with large κ_0 values were obtained. These results emphasize, once again, near-surface weathered zones attenuation effect at high frequencies.

From the engineering point of view, the sites which could be evaluated as reference sites were determined and also possible threats of the other sites with regard to seismic hazard assessments were emphasized, in this study. On the other hand, it would be highly desirable to measure near-surface structural complexities of the sites, even those located on hard rock sites. This would allow much more detailed interpretation of the origin of the observed spectral shapes.

Acknowledgments This paper is a part of a Ph.D. thesis undertaken by Tevfik Özgür Kurtulmuş at the Institute of Natural and Applied Sciences in Dokuz Eylül University (DEU). It is supported by DEU Scientific Research Foundation Grant BAP-Project No. 2008.KB.FEN.08. Figure 1 (after Akyol et al. (2013) includes the base maps from Çiftçi et al. (2010). Figure 2 was taken from Kurtulmuş and Akyol (2013). We thank the WASRE network team (Brian Mitchell, Lupei Zhu, Mike Fort, M. Ali Danışman, Oğuz Demir, Zülfikar Erhan, Adem Somer and Emre Timur) for their dedicated efforts during the data collection stage. We also thank Lupei Zhu, Aybige Akıncı, Sebastiano D'Amico and Murat Çamyıldız for their contributions during the data processing stages. We are grateful to Raul R. Castro for his precious comments on interpretation of the results. We would also like to thank the Editor Vladimir Schenk, Dino Bindi and an anonymous reviewer whose comments and suggestions significantly improved the manuscript.

References

Abercrombie RE, Leary P (1993) Source parameters of small earthquakes recorded at 2.5 km depth, Cajon Pass, southern California: implications for earthquake scaling. Geophys Res Lett 20:1511–1514

Akıncı A, D'Amico S, Malagnini L, Mercuri A (2013) Scaling earthquake ground motions in the western Anatolia, Turkey. Phys Chem Earth 63:124–135. doi:10.1016/j.pce.2013.04.013

Akyol N, Akıncı A, Eyidoğan H (2002) Separation of source, propagation and site effects from observed S-wave of Bursa City and its vicinity in the Northwestern Anatolian Fault Zone, Turkey. Pure Appl Geophys 159:1253–1269

Akyol N, Zhu L, Mitchell BJ, Sözbilir H, Kekovalı K (2006) Crustal structure and local seismicity in western Anatolia. Geophys J Int 166(3):1259–1269

Akyol N, Kurtulmuş TÖ, Çamyıldız M, Güngör T (2013) Spectral ratio estimates for site effects on the horst–graben system in west Turkey. Pure Appl Geophys 170(12):2107–2125. doi:10.1007/s00024-013-0661-2

Journal : Small 11069 | Dispatch : 12-2-2015 | Pages : 18
Article No. : 1660 | LE | TYPESET
MS Code : NHAZ-D-14-00285 | CP | DISK

Aldanmaz E (2006) Mineral–chemical constraints on the Miocene calc-alkaline and shoshonitic volcanic rocks of western Turkey: disequilibrium phenocryst assemblages as indicators of magma storage and mixing conditions. Turk J Earth Sci 15:47–73

Al-Lazki A, Sandvol E, Seber D, Barazangi M, Türkelli N, Mohamad R (2004) Pn tomographic imaging of mantle lid velocity and anisotropy at the junction of the Arabian, Eurasian and African plates. Geophys J Int 158:1024–1040

Anderson JG (1986) Implication of attenuation for studies of the earthquake source. In: Dag S, Boatwright J, Scholz CH (eds) Earthquake source mechanics, American Geophysical Union Monograph 37:311–318

Anderson JG, Hough SE (1984) A model for the shape of the Fourier amplitude spectrum of acceleration at high frequencies. Bull Seismol Soc Am 74(5):1969–1993

Andrews DJ (1986) Objective determination of source parameters and similarity of earthquakes of different size. In: Dag S, Boatwright J, Scholz CH (eds) Earthquake source mechanics, American Geophysical Union Monograph 37:259–267

Atkinson MG (1996) The high frequency shape of the source spectrum for earthquakes in eastern and western Canada. Bull Seismol Soc Am 86(1A):106–112

Bindi D, Parolai S, Grosser H, Milkereit C, Zünbül S (2006) Cumulative attenuation along source-to-receiver paths in Northwestern Turkey. Bull Seismol Soc Am 96(1):188–199

Boatwright J, Seekins LC, Fumal TE, Liu HS, Mueller CS (1991) Ground motion amplification in the Marina district. Bull Seismol Soc Am 81(5):1980–1997

Brune J (1970) Tectonic strain and the spectra of seismic shear waves from earthquakes. J Geophys Res 75:4997–5009

Castro RR, Anderson JG, Singh JG (1990) Site response, attenuation and source spectra of S waves along the Guerrero, Mexico, subduction zone. Bull Seismol Soc Am 80(6):1481–1503

Castro RR, Mungunia L, Brune JN (1995) Source spectra and site response from P and S waves of local earthquakes in the Oaxaca, Mexico, subduction zone. Bull Seismol Soc Am 85:923–936

Castro RR, Pacor F, Sala A, Petrungaro C (1996) S wave attenuation and site effects in the region of Friuli, Italy. J Geophys Res 101:22355–22369

Castro RR, Trojani L, Monachesi G, Mucciarelli M, Cattaneo M (2000) The spectral decay parameter κ; in the region of Umbria-Marche, Italy. J Geophys Res 105:23811–23823

Castro RR, Fabriol H, Bour M, Le Brun B (2003) Attenuation and site effects in the region of Guadeloupe, Lesser Antilles. Bull Seismol Soc Am 93(2):612–626

Castro RR, Pacor F, Bindi D, Franceschina G, Luzi L (2004) Site response of strong motion stations in the Umbria, central Italy region. Bull Seismol Soc Am 94(2):576–590

Çiftçi NB, Bozkurt E (2009) Evolution of the Miocene sedimentary fill of the Gediz graben, SW Turkey. Sediment Geol 216(3–4):49–79. doi:10.1016/j.sedgeo.2009.01.004

Çiftçi NB, Temel RO, İztan YH (2010) Hydrocarbon occurrences in the western Anatolian (Aegean) grabens, Turkey: is there a working petroleum system? AAPG Bull 94(12):1827–1857

Cornou C, Bard BY, Dietrich M (2003) Contribution of dense array analysis to identification and quantification of basin-edge induced waves. Part ii: application to Grenoble basin (French Alps). Bull Seismol Soc Am 93(6):2624–2648

Cotton F, Scherbaum F, Bommer JJ, Bungum H (2006) Criteria for selecting and adjusting ground-motion models for specific target regions: application to central Europe and rock sites. J Seismol 10:137–156

Douglas J, Gehl P, Bonilla LF, Gélis C (2010) A κ model for mainland France. Pure Appl Geophys 167:1303–1315

Drouet S, Cotton F, Gueguen P (2010) V_{S30}, κ, regional attenuation and Mw from accelerograms: application to magnitude 3–5 French earthquakes. Geophys J Int 182:880–898

Eyidoğan H, Akıncı A (1999) Site attenuation and source parameters on the North Anatolian Fault zone, eastern Turkey estimated from the aftershocks of 13 March 1992 Erzincan earthquake. J Seismol 3:363–373

Fernández AI, Castro RR, Huerta CI (2010) The spectral decay parameter kappa in northeastern Sonora, Mexico. Bull Seismol Soc Am 100(1):196–206. doi:10.1785/0120090049

Gentili S, Franceschina G (2011) High frequency attenuation of shear waves in the southeastern Alps and northern Dinarides. Geophys J Int 185:1393–1416

Gessner K, Ring U, Johnson C, Hetzel R, Passchier CW, Güngör T (2001) An active bivergent rollinhinge detachment system. Central Menderes metamorphic core complex in western Turkey. Geology 29:611–614

Göktürkler G, Şalk M, Sarı C (2003) Numerical modeling of the conductive heat transfer in western Anatolia. J Balkan Geophys Soc 6(1):1–15

Halldorsson B, Papageorgiou AS (2005) Calibration of the specific barrier model to earthquakes of different tectonic regions. Bull Seismol Soc Am 95:1276–1300

Journal : Small 11069 | Dispatch : 12-2-2015 | Pages : 18
Article No. : 1660 | LE | TYPESET
MS Code : NHAZ-D-14-00285 | CP | DISK

Hartzell SH (1992) Site response estimation from earthquake data. Bull Seismol Soc Am 82:2308–2327
Hetzel R, Passchier CW, Ring U, Dora OÖ (1995) Bivergent extension in orogenic belts: the Menderes Massif (southwestern Turkey). Geology 23:455–458
İlkışık OM (1995) Regional heat flow in western Anatolia using silica temperatures estimates from thermal springs. Tectonophysics 244:175–184
Iwakiri K, Hoshiba M (2012) High-frequency (>10 Hz) content of the initial fifty seconds of waveforms from the 2011 Off the Pacific coast of Tohoku earthquake. Bull Seismol Soc Am 102:2232–2238
Kilb D, Biasi G, Anderson JG, Brune J, Peng Z, Vernon FL (2012) A comparison of spectral parameter kappa from small and moderate earthquakes using southern California ANZA seismic network data. Bull Seismol Soc Am 102:284–300
Ktenidou OJ, Gelis C, Bonilla F (2013) A study on the variability of kappa in a borehole, implications on the computation method used. Bull Seismol Soc Am 103:1048–1068
Ktenidou OJ, Cotton F, Abrahamson NA, Anderson JG (2014) Taxonomy of κ: a review of definitions and estimations approaches target to applications. Seismol Res Lett 85(1):135–146
Kurtulmuş TÖ (2014) Investigation of source, site, regional and near surface attenuation characteristics in the western Anatolia region. In: PhD thesis, the faculty of engineering of Dokuz Eylül university, İzmir, Türkiye
Kurtulmuş TÖ, Akyol N (2013) Crustal attenuation characteristics in western Turkey. Geophys J Int 195(2):1384–1394. doi:10.1093/gji/ggt318
Le Pichon X, Chamot-Rooke C, Lallemant S, Noomen R, Veis G (1995) Geodetic determination of the kinematics of Central Greece with respect to Europe: implications for Eastern Mediterranean tectonics. J Geophys Res 100:12675–12690
Liu Z, Wuenscher ME, Herrmann RB (1994) Attenuation of body waves in the central New Madrid Seismic Zone. Bull Seismol Soc Am 84(4):1112–1122
Malagnini L, Akıncı A, Herrmann RB, Pino NA, Scognamiglio L (2002) Characteristics of the ground motion in northeastern Italy. Bull Seismol Soc Am 92(6):2186–2204
Malagnini L, Mayeda K, Akıncı A, Bragato PL (2004) Estimating absolute site effects. Bull Seismol Soc Am 94(4):1343–1352
Menke W (1989) Geophysical data analysis: discrete inverse theory. Academic Press, San Diego
Mutlu H (2007) Constraints on the origin of the Balıkesir thermal waters (Turkey) from stable isotope ($\delta^{18}O$, δD, $\delta^{13}C$, $\delta^{34}S$) and major-trace element compositions. Turk J Earth Sci 16:13–32
Mutlu AK, Karabulut H (2011) Anisotropic Pn tomography of Turkey and adjacent regions. Geophys J Int 187:1743–1758. doi:10.1111/j.1365-246X.2011.05235.x
Nakamura Y (1989) A method for dynamic characteristics estimations of subsurface using microtremors on the ground surface. Q Rep Railw Tech Res Inst (Japan) 30:25–33
Oth APH (2007) Source processes and spectral ground motion models of intermediate-depth Vrancea (Romania) earthquakes. In: PhD thesis, the faculty of physics of the university of Karlsruhe (TH), Karlsruhe
Oth A, Parolai S, Bindi D, Wenzel F (2009) Source spectra and site response from S waves of intermediate-depth Vrancea, Romania earthquakes. Bull Seismol Soc Am 99(1):235–254
Parolai S, Bindi D (2004) Influence of soil-layer properties on k evaluation. Bull Seismol Soc Am 94(1):349–356
Parolai S, Bindi D, Baumbach M, Grosser H, Milkereit C, Karakısa S, Zünbül S (2004) Comparison of different site response estimation techniques using aftershocks of the 1999 İzmit earthquake. Bull Seismol Soc Am 94(3):1096–1108
Petukhin AG, Irikura K (2000) A method for the separation of source and site effects and the apparent Q structure from strong motion data. Geophys Res Lett 27:3429–3432. doi:10.1029/2000GL011561
Purvance MD, Anderson JG (2003) A comprehensive study of the observed spectral decay in strong-motion accelerations recorded in Guerrero, Mexico. Bull Seismol Soc Am 93:600–611
Qin Y, Wang Y, Taneka H, Zhang X (2012) Seismic ground motion amplification in a 3D sedimentary basin: the effect of the vertical velocity gradient. J Geophys Eng 9:761–772. doi:10.1088/1742-2132/9/6/761
Rojay B, Toprak V, Demirci C, Süzen L (2005) Plio-Quaternary evolution of the Küçük Menderes graben southwestern Anatolia, Turkey. Geodin Acta 18(3–4):317–331
Sarı C, Şalk M (2006) Sediment thicknesses of the Western Anatolia graben structures determined by 2D and 3D analysis using gravity data. J Asian Earth Sci 26:39–48
Sayın A (2007) Origin of kaolin deposits: evidence from the Hisarcık (Emet-Kütahya) deposits, Western Turkey. Turk J Earth Sci 16:77–96
Seyitoğlu G, Işık V (2009) Meaning of the Küçük Menderes graben in the tectonic framework of the central Menderes metamorphic core complex (western Turkey). Geol Acta 7(3):323–331

Journal : Small 11069 | Dispatch : 12-2-2015 | Pages : 18
Article No. : 1660 | LE | TYPESET
MS Code : NHAZ-D-14-00285 | CP | DISK

Tarcan G, Filiz S, Gemici U (2000) Geology and geochemistry of the Salihli geothermal fields, Turkey. World Geothermal Congress, Kyushu-Tohoku, Japan, pp 1829–1834

Taymaz T, Jackson J, McKenzie D (1991) Active tectonics of the North and Central Aegean Sea. Geophys J Int 106:433–490

Tokçaer M, Agostini S, Savasçın MY (2005) Geotectonic setting and origin of the youngest Kula volcanics (western Anatolia), with a new emplacement model. Turk J Earth Sci 14:145–166

Tsai C-CP, Chen K-C (2000) A model for the high-cut process of strong motion accelerations in terms of distance, magnitude, and site condition: an example from the SMART 1 array, Lotung, Taiwan. Bull Seismol Soc Am 90:1535–1542

Yalçınkaya E, Tekebaş S, Pınar A (2013) Analysis of ambient noise in Yalova, Turkey: discrimination between artificial and natural excitations. J Seismol 17:1021–1039. doi:10.1007/s10950-013-9370-7

Yılmaz H (2007) Stream sediment geochemical exploration for gold in the Kazdağ dome in the Biga peninsula, Western Turkey. Turk J Earth Sci 16:33–55

Zhu L, Akyol N, Mitchell BJ, Sözbilir H (2006) Seismotectonics of Western Turkey from high resolution earthquake relocations and moment tensor determinations. Geophys Res Lett 33:L07316. doi:10.1029/2006gl025842